

LARGE SCALE STRUCTURES IN THE EARLY SDSS: COMPARISON OF THE NORTH AND SOUTH GALACTIC STRIPS

ENRIQUE GAZTAÑAGA^{a,b}

^a INAOE, Astrofísica, Tonantzintla, Apdo Postal 216 y 51, Puebla 7200, Mexico

^bInstitut d'Estudis Espacials de Catalunya, ICE/CSIC, Edf. Nexus-104-c/Gran Capita 2-4, 08034 Barcelona, Spain

Draft version December 2, 2024

ABSTRACT

We compare the large scale galaxy clustering in the North and South SDSS early data release (EDR) with the clustering in the APM Galaxy Survey. The three samples are independent and cover an area of 150, 230 and 4300 square degrees respectively. We combine SDSS data in different ways to approach the APM selection. Given the good photometric calibration of the SDSS data and good match of its North and South number counts, we combine them in a single sample. The joint clustering is compared with equivalent subsamples in the APM. The resulting errors are small enough to test some of the results in the APM. We find some evidence for an inflection in the shape of $w_2(\theta)$, which can be interpreted as the result of weakly non-linear gravitational growth. We can also confirmed good agreement with the hypothesis of Gaussian initial conditions (and small biasing) for the structure traced by the large scale SDSS galaxy distribution.

Subject headings: g

galaxies: clustering, large-scale structure of universe

1. INTRODUCTION

The SDSS collaboration have recently made an early data release (EDR) publicly available. This contains around a million galaxies distributed within a narrow strip of 2.5 degrees across the equator. As the strip crosses the galactic plane, the data is divided into two separate sets in the North and South Galactic caps. The SDSS collaboration has presented a series of analysis (Scranton etal 2001, Connolly etal 2001, Dodelson etal 2001, Tegmark etal 2001, Szalay etal 2001) of angular clustering centered on the North Galactic strip, which contains the best seeing conditions. Gaztanaga (2001, hereafter G01) presented a study of bright ($g' \simeq 20$) SDSS galaxies in the South Galactic EDR strip, centering the analysis on the comparison of clustering to the APM Galaxy Survey (Maddox etal 1990).

In this paper we want to compare and combine the bright ($r' \simeq 19$ or $g' \simeq 20$) galaxies in North and South strips to make a more detailed and precise comparison to the APM. Do the North and South strips have similar clustering? How do they compare to previous analysis? Answering these questions would help us understanding the SDSS EDR data and, at the same time, will give us the opportunity to test how reliable are earlier conclusions drawn from the APM analysis. In particular regarding the shape of the 2-point function (Maddox etal 1990, Gaztañaga & Juszkiewicz 2001) and higher order correlations (eg Frieman & Gaztañaga 1999 and references therein).

This paper is organized as follows. In section §2 we present the samples used and the galaxy selection and number counts. Section §3 shows the comparison of the 2 and 3-point correlation functions. We end with some discussion and a listing of conclusions.

2. SDSS SAMPLES AND PIXEL MAPS

We follow the steps described in Gaztanaga (2001, hereafter G01). We download data from the SDSS public archives using the SDSS Science Archive Query Tool (sdssQT, <http://archive.stsci.edu/sdss/software/>). We select objects from an equatorial SGC (South Galactic Cap) strip 2.5 wide ($-1.25 < DEC < 1.25$ degrees.) and 66 deg. long ($351 < RA < 56$ deg.), which will be called EDR/S, and also from a similar NGC (North Galactic Cap) 2.5 wide and 91 deg. long ($145 < RA < 236$ deg.), which will be called EDR/N. These strips (SDSS numbers 82N/82S and 10N/10S) correspond to some of the first runs of the early commissioning data (runs 94/125 and 752/756) and have variable seeing conditions. Runs 752 and 125 are the worst with regions where the seeing fluctuates above 2". Runs 756 and 94 are better, but still have seeing fluctuations of a few tenths of arc-second within scales of a few degrees¹. These seeing conditions could introduce large scale gradients because of the corresponding variations in the photometric reduction (eg star-galaxy separation) that could manifest as large scale number density gradients (see Scranton et al 2001 for a detailed account of these effects). We will test our results by restricting the analysis to runs 756 and 94, which should be less affected by this possible systematics from seeing.

We further consider a sample which includes both the North and South strips, this will be called: EDR/(N+S). Note that the clustering from this sample will not necessarily agree with the mean of EDR/N and EDR/S (eg $EDR/(N+S) \neq EDR/N + EDR/S$).

We first select all galaxies brighter than $u' = 22.3, g' = 23.3, r' = 23.1, i' = 22.3, z' = 20.8$, which corresponds to the SDSS limiting magnitudes for 5 sigma detection in

¹See <http://www-sdss.fnal.gov:8000/skent/seeingStatus.html> or Figure 4 in Scranton etal 2001

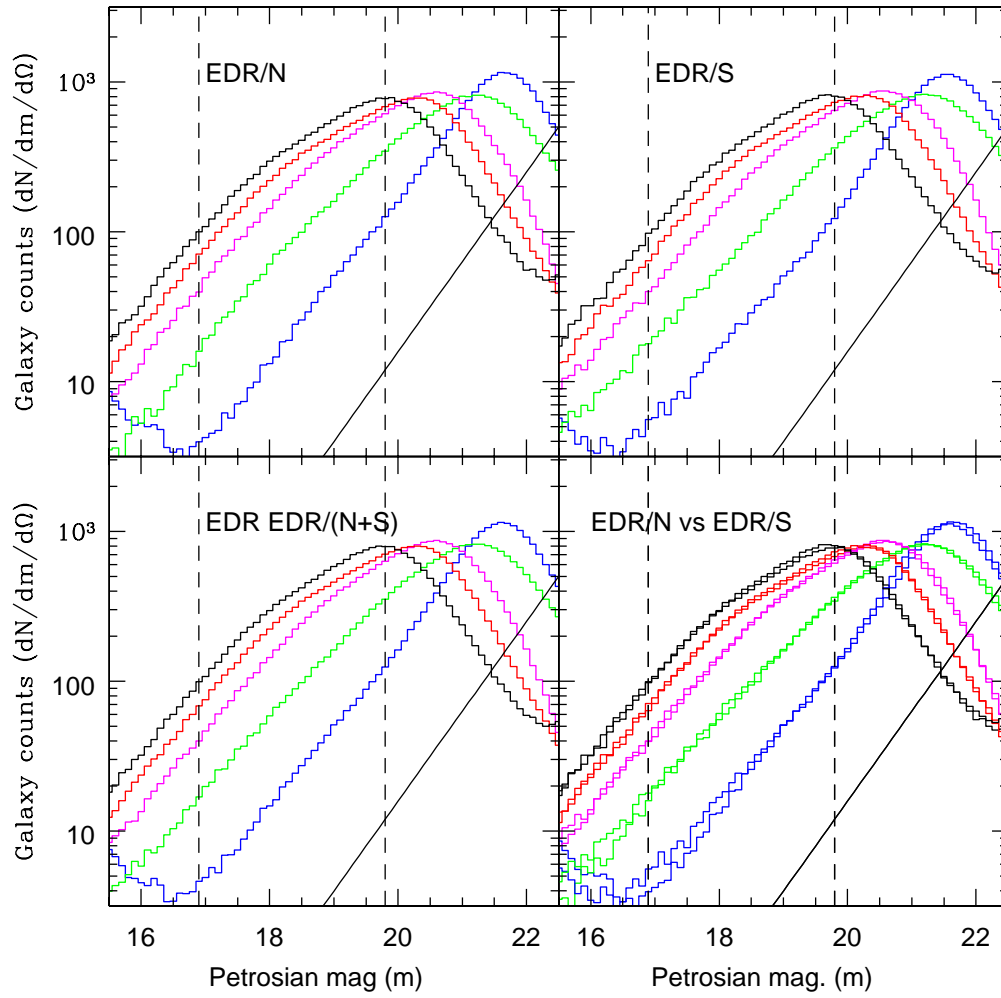


FIG. 1.— Galaxy density counts per magnitude bin and square deg. $dN/dm/d\Omega$ as a function of Petrosian magnitude z', i', r', g', u' (from left to right). The top panels show EDR/N (left) and EDR/S (right). The bottom left panel shows EDR/(N+S) while the right panel compares EDR/S to EDR/N.



FIG. 2.— Pixel maps of equatorial projections of EDR/N (top) with 2.5×90 sqr.deg. and EDR/S (bottom) with 2.5×60 sqr.deg.

point sources (York et al. 2000). Galaxies are found from either the 1×1 , 2×2 or 4×4 binned CCD pixels and they are de-blended by the SDSS pipeline (Lupton et al 2001). Only isolated objects, child objects and objects on which the de-blender gave up are used in constructing our galaxy catalog (see Yasuda et al 2001).

There are about 375000 objects classified as galaxies in the EDR/S and about 504000 in the EDR/N. Figure 1 shows the number counts (surface density) for all these 879000 galaxies as a function of the magnitude in each band, measured by the SDSS modified Petrosian magnitudes m'_u , m'_g , m'_r , m'_i and m'_z (see Yasuda et al 2001 for a discussion of the SDSS counts). Continuous diagonal lines show the $10^{0.6m}$ expected for a low redshift homogeneous distribution with no k-correction, no evolution and no-extinction.

We next select galaxies with SDSS modified Petrosian magnitudes to match the APM selection. We try different prescriptions. We first apply the following transformation to try to mimic the APM filter B_J :

$$B_J = g' + 0.193(g' - r') + 0.115 \quad (1)$$

This results from combining the relation $B_J = B - 0.28(B - V)$ (Maddox et al 1990) with expressions (5) and (6) in Yasuda et al (2001). As the mean color $g' - r' \simeq 0.7$ the above relation gives a mean $B_J \simeq g' + 0.25$, which roughly agrees with the magnitude shift used in G01. For the $17 < B_J < 20$ range (using the above transformation) we find $N \simeq 123000$ galaxies in the EDR/(N+S), with a galaxy surface which is very similar to the one in the APM (only 5% larger after subtraction of the 5% star-merger contribution in the APM). In any case this type of color transformations between bands are not very accurate as they only work in some average statistical sense. The uncertainties are even stronger when we recall that the APM uses fix isophotal aperture, while SDSS is using Petrosian magnitudes, a difference that can introduce additional color terms and surface brightness dependence.

It is much cleaner to use a single SDSS band. We should use g' which is the closest to the APM $\lambda_{B_J} \simeq 4200$ ($\lambda_u \simeq 3560$, $\lambda_{g'} \simeq 4680$ and $\lambda_{r'} \simeq 6180$). But how do we decide the range of g' to match the APM $17 < B_J < 20$? We try two approaches. One is to look for the magnitude interval that has the same counts, as done in G01. The resulting range is $16.8 < g' < 19.8$. This gives a reasonable match to the clustering amplitudes in the EDR/S and EDR/N. But there is no reason to expect a perfect match: the selection function and resulting depth is different for different colors. The other approach is to fix it to the same magnitude range, ie $17 < g' < 20$, rather than the same counts. This produces $N \simeq 157000$ galaxies, which corresponds $\simeq 25\%$ higher counts than the APM. This does not necessarily mean that this sample is deeper than the APM, because of the intrinsic different in color selection, K-corrections and possible color evolution.

Finally, we produce equal area projection pixel maps of various resolutions similar to those made in G01. Except for a few tests, all the analysis presented here correspond to $3'.5$ resolution pixels. On making the pixel maps we mask out about 1.75 of the EDR sample from the edges, which makes an integer number of pixels in our equatorial projection. This also avoids potential problem of the

galaxy photometry on the edges (although higher resolution maps show very similar results, indicating that this is not really a problem).

2.1. Galactic extinction

The above discussion ignored Galactic extinction. It should be noted that the standard extinction law $A_b = C(\csc b - 1)$ with $C = 0.1$ was used for the APM photometry. This is a very small correction: $A_b = 0$ at the poles ($b = 90$ deg) and the maximum $A_b \simeq 0.03$ at the lowest galactic declination ($b \simeq 50$ deg). This is in contrast to the Schlegel et al (1998) extinction maps which have significant differential extinction $E(B - V) \simeq 0.02 - 0.03$ even at the poles. The corresponding total absorption A_b for the B_J band according to Table 6 in Schlegel et al (1998) is four times larger: $A_b \simeq 0.08 - 0.12$. This increases up to $A_b \simeq 0.2 - 0.3$ at galactic declination $b \simeq 50$. Using the Schlegel et al (1998) extinction correction has a large impact in the number counts shifting the mean magnitude ranges by $\simeq 0.2$ magnitudes for the EDR samples. Thus, it is important to know what extinction correction has been applied when comparing different surveys or magnitude bands.

Despite the possible impact on the quoted magnitudes (and therefore counts), extinction has little impact on clustering, at least for $r' < 21$ (see Scranton et al 2001 and also Tegmark et al 1998). This is fortunate because of the uncertainties involved in making of the extinction maps and its calibration. Moreover, the Schlegel et al (1998) extinction map only has a $6'.1$ FWHM, which is much larger than the individual galaxies we are interested on. Many dusty regions have filamentary structure (with a fractal pattern) and large fluctuations in extinction from point to point. One would expect similar fluctuations on smaller (galaxy size) scales, which introduces further uncertainties to individual corrections.

Here we decided not to correct for extinction, as this will be closer to the APM analysis and makes little effect on clustering at the depths and for the issues that will be explored here. We have double checked this by applying the Schlegel et al (1998) extinction correction to one of our low resolution maps in B_J (assuming a ratio of total to selective extinction of $R_{B_J} \simeq 4$).

To avoid confusion with other prescriptions by the SDSS collaboration we will use z', i', r', g', u' for 'raw', uncorrected magnitudes, and z^*, i^*, r^*, g^*, u^* for extinction corrected magnitudes. For example, according to Schlegel et al (1998) $r' = 18$ corresponds roughly to an average extinction corrected $r^* \simeq 17.9$ for a mean differential extinction $E(B - V) \simeq 0.03$.

3. CLUSTERING COMPARISON

To study sampling and biasing effects on the SDSS clustering estimators we have cut different SDSS-like strips out of the APM map (see G01). For the APM, we have considered a $17 < B_J < 20$ magnitude slice in an equal-area projection pixel map with a resolution of 3.5 arc-min, that covers over 4300 deg^2 around the SGC. The APM sample can fit about 25 strips similar to EDR/S and 16 similar to EDR/N. The APM can not cover the combined EDR/(N+S) as it extends across the whole equatorial circle. But we can place 2 strips similar to EDR/S and EDR/N well separated, eg by at least 10 degrees, within

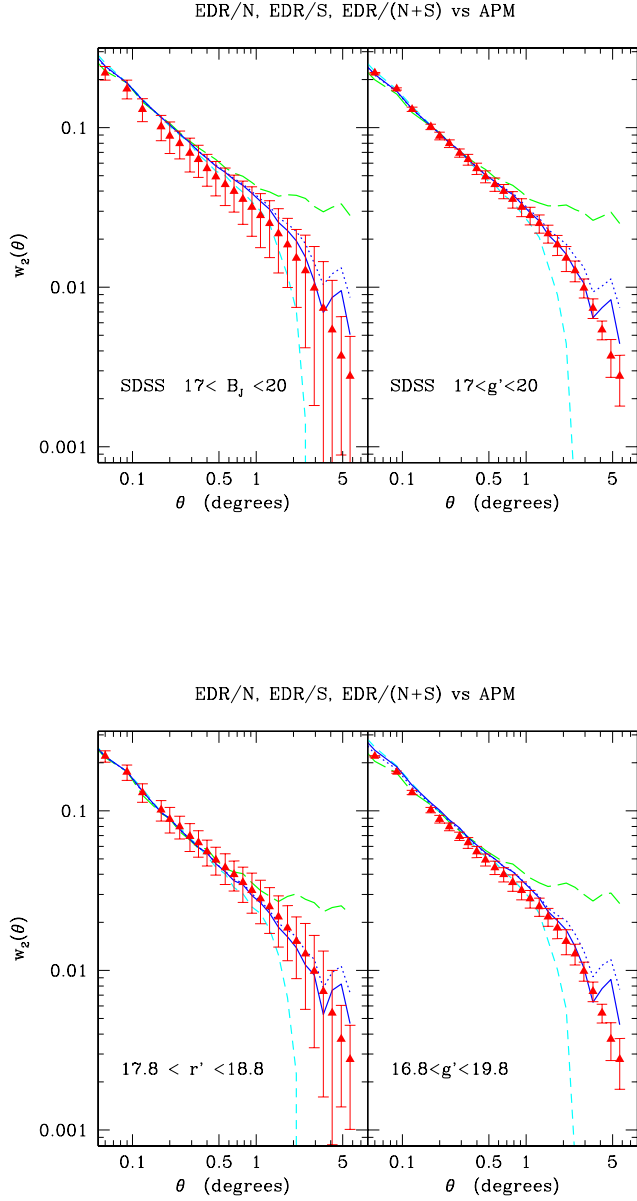


FIG. 3.— The angular 2-point function $w_2(\theta)$ as a function of galaxy separation θ for different SDSS magnitudes as labeled in the figures. The short and long dashed lines correspond to the SDSS EDR/N (North) and EDR/S (South) strips. The continuous line corresponds to EDR/(N+S), a joint analysis of the SDSS South and North data. The dotted line is the mean of the EDR/N and EDR/S. The triangles with errorbars show the mean and 1-sigma confidence level in the values of 10 APM sub-samples that simulate the different EDR samples: EDR/S (errors in the first panel), EDR/(N+S) (error in second and fourth panels) and EDR/S (errors in third panel).

the APM map. As correlations are negligible on angular scales > 10 degrees, this simulates well the combined EDR/(N+S) analysis. To study sampling effects over individual scans we also extract individual SDSS-like CCD scans out of the APM pixel maps. In all cases we correct the clustering in the APM maps for a 5% contamination of randomly merged stars (see Maddox et al 1990), ie we scale fluctuations up by 5% (see also Gaztañaga 1994).

3.1. The angular 2-point function

We first study the angular two-point function. Figure 3 shows the results from the EDR/S (long-dashed), EDR/N (short-dash) and EDR/(N+S) (continuous lines). As mentioned above, the clustering from the combined sample EDR/(N+S) will not necessarily agree with the mean of EDR/N and EDR/S (shown as dotted lines) for several reasons: estimators are not linear, neither are sampling errors and local galaxy fluctuations are estimated around the combined mean density (rather than the mean density in each subsample). As shown in Figure 3 the two estimators are indeed different. In general for a well calibrated survey the whole, ie EDR/(N+S), should give better results than the sum of the parts, so that we take the EDR(N+S) results as our best estimate.

The results for EDR/N in Figure 3 agree well with the corresponding comparison in Fig.1 of Connolly et al (2001) for the r' SDSS filter. The results for EDR/S agree with G01. Our results for $16.8 < g' < 19.8$ (chosen to match the APM surface density, as in G01) are shown in the third panel of Figure 3 and give intermediate results between the B_J and g' in Figure 3.

The EDR/(N+S) results for $17 < g' < 20$ (second panel) agree very well with the APM data (triangles). Note that here the errorbars in the APM correspond to subsamples of similar size and shape as the EDR/(N+S). The results for EDR/(N+S) $17 < B_J < 20$ (shown in the first panel) are about 15% higher in amplitude than the APM. As mentioned above this is not totally surprising as the magnitude conversion should only work on some average sense.

Note that Scranton et al 2001 studied the SDSS systematic effects with r^* colors, and found that most of the (masked) systematic effects had negligible contributions to $w_2(\theta)$ for $r^* < 21$ (eg see their figure 15). The APM $B_J \simeq 17 - 20$ has a depth corresponding to $r^* \simeq 18.5$, which is almost 3 magnitudes brighter than the limit where systematics seem important. We further study the $w_2(\theta)$ shape in r' . The brighter sample of $r^* = 18 - 19$ in Connolly et al (2001) is slightly deeper than the APM, with $z \simeq 0.18$ (Connolly et al 2001) rather than $z \simeq 0.15$ for the APM (Maddox et al 1990). We find that $r' = 17.8 - 18.8$ is the closer one magnitude r' bin in depth, because of the average extinction this corresponds roughly to extinction corrected $r^* = 17.65 - 18.65$ in Connolly et al (2001). It turns out that the $r' = 17.8 - 18.8$ also matches very well the $B_J \simeq 17 - 20$ APM $w_2(\theta)$ amplitude. The SDSS $17.8 < r' < 18.8$ sample has about 40% less galaxies (per square degree) than the APM, presumably because of the color correction and differences in the photometric selection. Results for this r' sample are shown in the 3rd panel (second from the right) in Figure 3 and are compared to the APM subsamples similar to EDR/N (note how they are slightly smaller than the errors in the APM shown in the first panel of Figure 3, as expected from the smaller

area of EDR/S).

3.2. $w_2(\theta)$ in central scans 756 and 94

As a further test for systematic, we study $w_2(\theta)$ using only the central region of the CCD in scans 756 (North EDR) and 94 (South EDR). The seeing during run 756 is the best in the EDR with only small fluctuations around $1''.4$. Regions in the SDSS where the seeing degraded to worse than $1''.5$ are marked for re-observations. As this includes most of the EDR data one may be worry that some of the results presented here are affected by this seeing variations. As mentioned above this has been shown not to be the case, at least for $r^* < 21$ (Scranton et al 2001).

We estimate $w_2(\theta)$ using only galaxies in the central regions of the CCD in scans 756 (the best of EDR/N) and 94 (the best of EDR/S). Figure 4 shows a piece of this new data set for the EDR/N. As can be seen in the figure (bottom panel) we only consider the central part of 756 to avoid any contamination from the CCD edges. The new data set with the scans contains only 30% of the area (and of the galaxies) from the whole strip.

Figure 5 compares the results of $w_2(\theta)$ for the individual scans against the whole strip for all EDR/S, EDR/N and EDR/(N+S). As can be seen in this Figure, individual scans (dotted lines) agree very well with the corresponding overall strip values. Systematic errors seem small, and in fact the agreement is striking after a visually comparison of the heavy masking in the pixel maps of Figure 4 (which shows the actual resolution use for the $w_2(\theta)$ estimation in Fig. 5). One would naively expect some more significant sampling errors when we use only 1/3 of the data. But nearby regions are strongly correlated and we can get very similar results with only a fraction of the data (this is also nicely shown in Figures 13-15 of Scranton et al 2001). This test shows the power of doing configuration space analysis (as opposed to Fourier space analysis). It also illustrates that our estimator for $w_2(\theta)$ performs very well on dealing with masked data.

3.3. An inflection point in $w_2(\theta)$?

Figure 5 shows the logarithmic slope:

$$\gamma(r) = \frac{d \log w_2(\theta)}{d \log \theta} \quad (2)$$

of $w_2(\theta)$ in the right panel Fig.3 and Fig.5

The errors in the top panel correspond to the EDR/S strip. Within these errors, both the APM and SDSS data are compatible with a power law $w_2(\theta) \simeq \theta^\gamma$ with γ between $\gamma \simeq -0.6$ and $\gamma \simeq -0.8$ (shown as two horizontal dotted lines), in good agreement with Table 1 in Connolly et al (2001) and Maddox (1990). Even with this large errors there is a hint of a systematic flattening of γ between 0.1 and 1.0 degrees in all subsamples. This hint is clearer in the combined analysis EDR/(N+S) where the errors (according to the APM subsamples) are significantly smaller. This flattening, of only $\Delta\gamma \simeq 0.1 - 0.2$ as we move from 0.1 to 1.0 degrees, is apparent in all the APM and SDSS subsamples. It is also reassuring that even at this detailed level all data agree within the errors. It is also apparent from the top panel of Fig.5 that the errors are too large to detect this effect in the EDR/N sample studied in Connolly et al (2001).

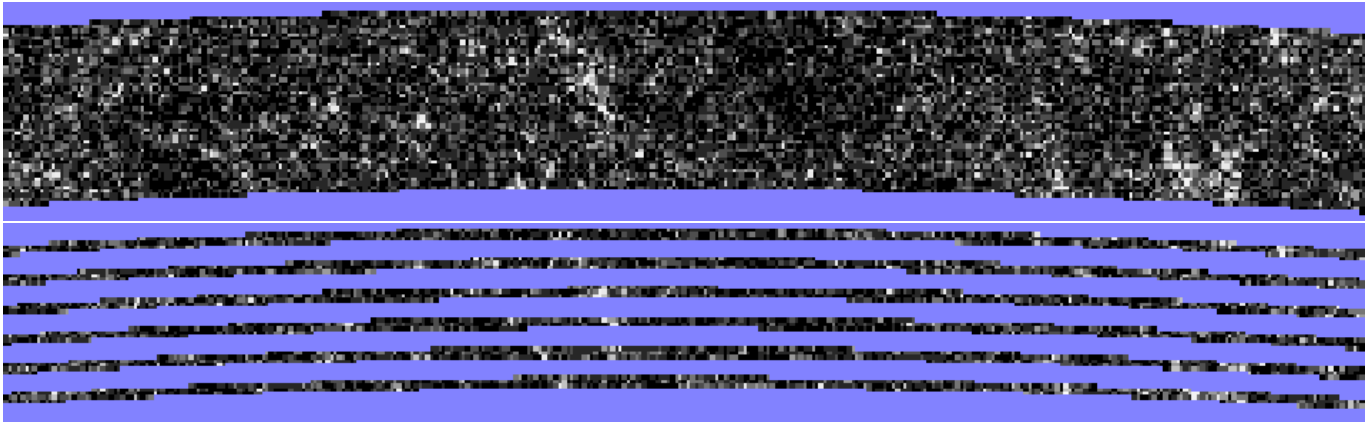


FIG. 4.— Pixel maps of a small part (2.5×18 sq.deg.) of the central region of the EDR/N strip (10N/10S) with the full 752+756 overlapping runs (top) and the same region view with the central 6 CCD regions is run 756. Note that with this resolution (3'.5) a single CCD field is only a few pixels wide.

As we have not estimated the full covariance matrix it is still difficult to assess a precise significance for this effect. We leave this to future studies (and more SDSS data). It is nevertheless clear that the γ data is better fit with a tilt in γ , which gives a maximum for γ . We will return to this point in the discussion.

3.4. Smoothed 1-point Moments

We next compare the lower order moments of counts in cells of variable size θ (larger than the pixel map resolution). We follow closely the analysis of G01. Fig. 6 shows the variance of fluctuations in density counts $\delta \equiv \rho/\bar{\rho} - 1$ smoothed over a scale θ : $\bar{w}_2 \equiv \langle \delta^2(\theta) \rangle$, which is plotted as a function of the smoothing radius θ . The errors show 1-sigma confidence interval for APM subsamples with EDR/(N+S) size. The individual results in each subsample are strongly correlated so that the whole curve for each subsample scales up and down inside the errors, ie there is a strong covariance at all separations due to large scale density fluctuations. The EDR/(N+S) results (continuous line) match perfectly the APM results, in agreement to what we found for the 2-point function above. The size of the errorbars for EDR/N and EDR/S are almost a factor of two larger than for EDR/(N+S), so that they are also in agreement with the APM within their respective sampling errors.

Left panel of Fig. 6 shows the corresponding comparison for the normalized angular skewness:

$$s_3(\theta) \equiv \frac{\langle \delta^3(\theta) \rangle}{\langle \delta^2(\theta) \rangle^{3/2}} \equiv \frac{\bar{w}_3(\theta)}{\bar{w}_2(\theta)} \quad (3)$$

All SDSS g' color sub-samples (top panel) for s_3 show an excellent agreement with the APM at the smaller scales (in contrast with the EDSGC results, see Szapudi & Gaztañaga 1998). On larger scales the SDSS values are smaller, but the discrepancy is not significant given the strong covariance of individual APM subsamples.

Bottom panel of the left of Fig. 6 shows the corresponding results in r' . At the smallest scale (of about 2' or 240 Kpc/h) we find some slight discrepancies (at only 1-sigma level for a single point) with the APM. The r' results seem a scaled up version of the g' results, which indicates that the apparent differences can be explained in terms of sampling effects (with strong covariance). Note also that the

value of s_3 seems to peak at slightly larger scale. This could hint to another component for this discrepancy. Szapudi & Gaztañaga 1998 argued that such peak could be related to some systematic (or physical) problem (issue) regarding the de-blending of large galaxies. It is reasonable to expect that such effect could be strong function of color, as g' and r' trace different aspects of the galaxy morphology. We have also checked that results of individual scans 756 and 94 (and also 756+94) are slightly higher, closer to the r' results than to the mean g' .

Similar results are found for higher order moments. As we approach the scale of 2 degrees, the width of our strip, it becomes impossible to do counts for larger cells and it is better to study the 3-point function.

3.5. 3-point Correlation function

Following G01 we next explore the 3-point function, which is normalized as:

$$q_3 \equiv \frac{w_3(\theta_{12}, \theta_{13}, \theta_{23})}{w_2(\theta_{12})w_2(\theta_{13}) + w_2(\theta_{12})w_2(\theta_{23}) + w_2(\theta_{13})w_2(\theta_{23})} \quad (4)$$

where θ_{12} , θ_{13} and θ_{23} correspond to the sides of the triangle form by the 3 angular positions of $\delta_1 \delta_2 \delta_3$. Here we will consider isosceles triangles, ie $\theta_{12} = \theta_{13}$, so that $q_3 = q_3(\alpha)$ is given as a function of the interior angle α which determines the other side of the triangle θ_{23} (FG99). We also consider the particular case of the collapsed configuration $\theta_{23} = 0$, which corresponds to $\langle \delta_1 \delta_2^2 \rangle$ and is normalized in slightly different way (see also Szapudi & Szalay 1999):

$$c_{12} \equiv \frac{\langle \delta_1 \delta_2^2 \rangle}{\langle \delta_1 \delta_2 \rangle \langle \delta_1^2 \rangle} \simeq 2q_3(\alpha = 0) . \quad (5)$$

Figure 7 shows c_{12} from the collapsed 3-point function.

Note the strong covariance in comparing the EDR/N to EDR/S. The EDR/(N+S) results agree very well with the APM within errors. We find similar results for the individual scans discussed above.

Left panel in Fig. 7 shows the reduced 3-point function q_3 for isosceles triangles of side $\theta_{12} = \theta_{13} = 0.5$ degrees. Here there seems to be a systematic difference between APM and SDSS, but its significance could be low

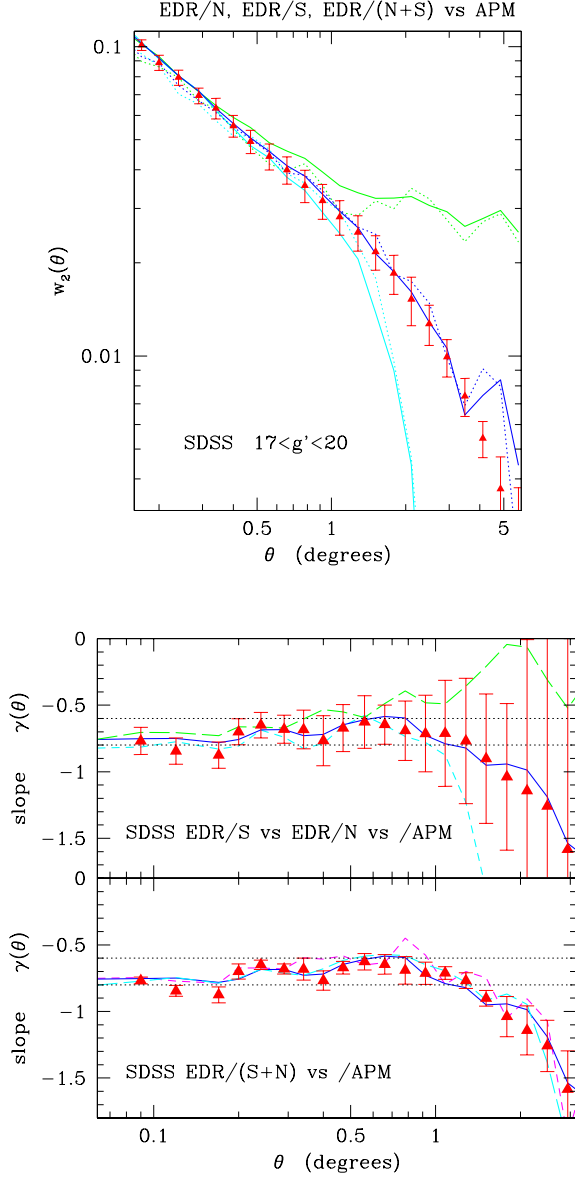


FIG. 5.— LEFT PANEL: Zoom over a region of the second panel of Figure 3. Here we compare the full strips of EDR/S, EDR/N and EDR/(N+S) (continuous lines from top to bottom at the largest angles) as compare with the APM subsamples (triangle with errorbars) of size similar EDR/(N+S). The dotted lines correspond to the central part of the CCD in scans 126 (top dotted line, next to EDR/S), 756 (bottom, next to EDR/N) and the joint 756+126 (middle dotted line, along EDR/(N+S)).

RIGHT PANEL: Logarithmic slope of the angular 2-point function $\gamma(\theta)$ as a function of galaxy separation θ for SDSS. The lines in the top panel correspond to the ones in the second panel of Fig.3 (ie EDR/S, EDR/N and EDR/(N+S)). In the bottom panel we also show the EDR/(N+S) in the corrected $17 < B_J < 20$ (short dashed line), again $17 < g' < 20$ (continuous line) and the central region of the CCDs in scans 756+94 (long dashed line). The triangles with errorbars show the mean and 1-sigma confidence level in the values of several APM sub-samples similar to EDR/(N+S). The errorbars in the top panel corresponds to EDR/S. The horizontal dotted lines shows $\gamma = -0.6$ and $\gamma = -0.8$.

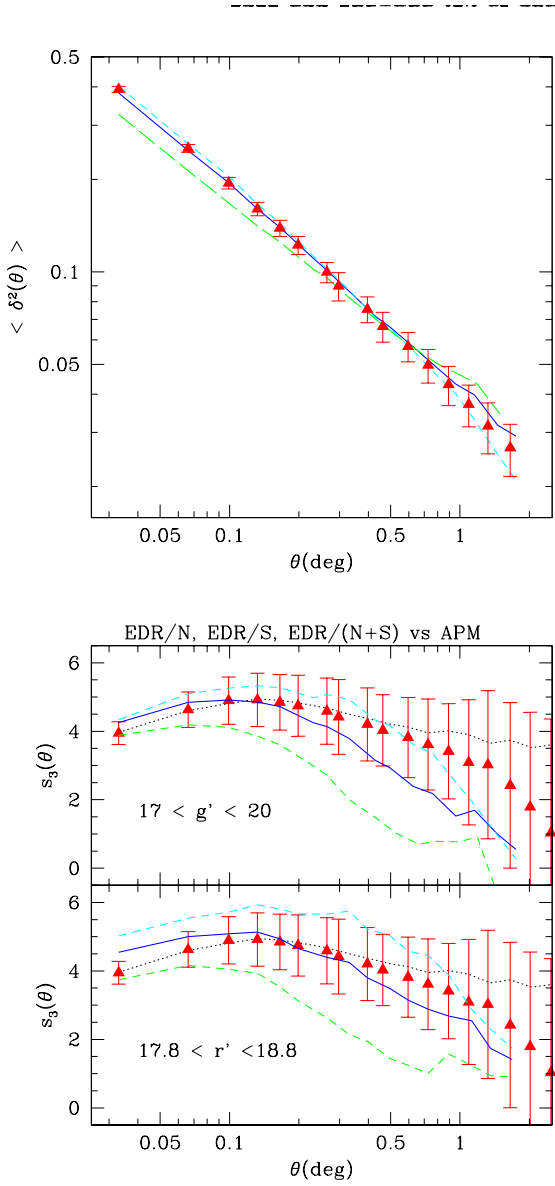


FIG. 6.— LEFT PANEL: The variance \bar{w}_2 as a function of angular smoothing θ . Short dashed, long dashed and continuous lines correspond to the SDSS EDR/N, EDR/S and EDR/(N+S). The points with errorbars show the mean and 1-sigma confidence level in the values of 10 APM sub-samples with same size and shape as the EDR/(N+S). RIGHT PANEL: same results for the reduced skewness s_3 . The top and bottom panel show the results in g' and r' .

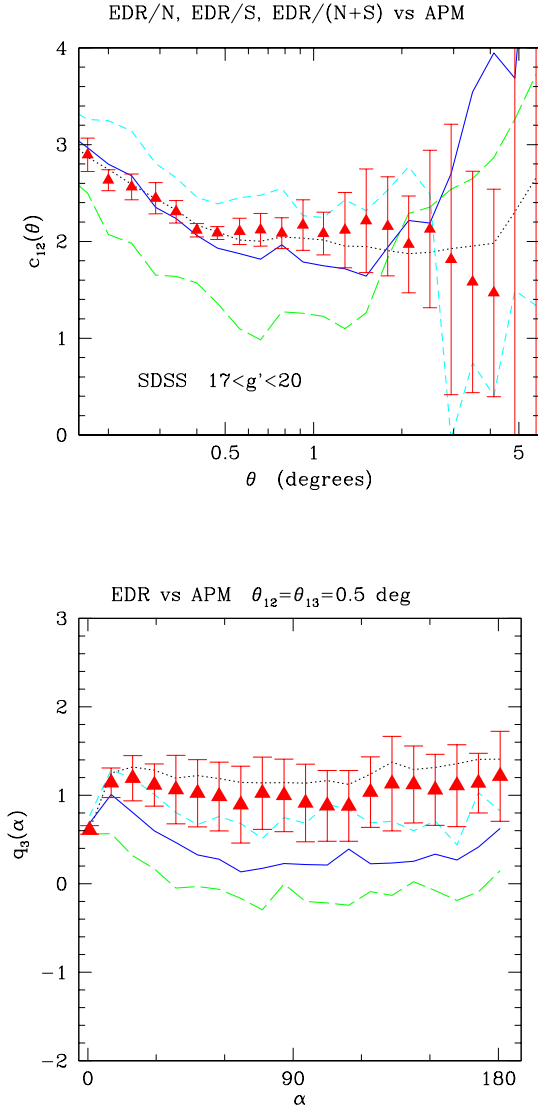


FIG. 7.— LEFT PANEL: The collapse 3-point function c_{12} as a function of galaxy separation θ for SDSS $17 < g' < 20$. The short and long dashed lines correspond to the SDSS EDR/N (North) and EDR/S (South) strips. The continuous line corresponds to EDR/(N+S). The triangles with errorbars show the mean and 1-sigma confidence level in the values of 10 APM sub-samples ($17 < B_J < 20$) with same size as the joint EDR/(N+S).
 RIGHT PANEL: Similar result for the 3-point function $q_3(\alpha)$ in isosceles triangles of side $\theta_{12} = \theta_{13} = 0.5$ deg.

if we recall that the errors at a single point is 1-sigma and that there is a strong covariance between points (eg note how the EDR/S and EDR/N curves shift around the EDR(N+S) one). The APM seems more compatible with the EDR/N. This is a tendency that is apparent in previous figures, but it is only on q_3 where the discrepancies starts to look significant.

4. DISCUSSION AND CONCLUSIONS

We have first explored the different uncertainties involved in the comparison of the SDSS with the APM. Which band to used? what magnitude range? After several test, we conclude that clustering in both the North and South EDR strips (EDR/N and EDR/S) agree well in amplitude and shape with the APM on scales $\theta < 2$ degrees. But we find inconsistencies with the APM $w_2(\theta)$ at the level of 90% significance on any individual scale at $\theta > 2$ degrees. This inconsistencies are even larger when we compare EDR/S to EDR/N. This is in agreement with the preliminary study in G01. Given the strong covariance between points it is difficult to asses how much bigger is the significance level for the whole $w_2(\theta)$ curve. We have also shown that this is probably not related to systematic photometric errors due to seeing variations across the SDSS EDR. We find similar results when using only 1/3 of the strip corresponding to the central part of the CCDs in the best scans (see Fig.5). So what is the reason for this apparent disagreement between the individual EDR/N and EDR/S strips, given the APM errors? One possible source of uncertainty is the accuracy of the APM calibration across 60 or 90 degrees RA strips (and fixed declination intervals), which could be lower than the accuracy on individual plates. Note that we are talking about fluctuations on scales of hundreds of Mpc/h. Even if these uncertainties have little effect on the APM estimation of $w_2(\theta)$ on scales $\theta < 10$ degrees, they could give inaccurate result for the sampling errors of 60-90 degree strips. As we approach the width of the APM survey one would expect that the APM plate matching procedure should smooth out real density gradients, which are constraint to be zero on the scale of the survey. Thus, it is not clear that the APM errors are accurate to asses the discrepancies at this level. We have tried to checked this point with APM-like mock maps drawn from the Nbody simulations presented in Gaztanaga & Baugh (1998). We find that the corresponding sampling errors could indeed be slightly larger in some cases that the ones estimated from the APM subsamples. The problem here is that we have to blindly trust the (dark matter) Nbody simulations on scales of hundreds of Mpc/h, where observational uncertainties on the fluctuation levels are large. Moreover, the Nbody simulations could also suffered from volume effect on such scales. More work is needed to assess these effects more carefully.

We have pushed the comparison further by combining the North and South strips, which we call EDR/(N+S) and analyze the EDR clustering as a whole. Combining samples in such a way is very risky with standard surveys because small systematic differences in the photometry tend to introduce large uncertainties in the overall mean surface density. This was overcome in the APM by a simultaneous match of many overlapping plates. For non-contiguous surveys the task is almost impossible, unless one has very well calibrated photometric observations,

as it is the case for the SDSS, to a level of 0.03 magnitudes (see Luton etal 2001). The combined EDR/(N+S) sample shows very good agreement for the number counts (see Figure ??) and also with the APM $w_2(\theta)$, even at $\theta > 2$ degrees. In this case the agreement is in fact within the corresponding sampling errors in the APM. This indicates that the indeed the discrepancies found in either EDR/N or EDR/S are due to sampling (rather than systematic) errors.

Higher order correlations show similar results. The mean SDSS skewness is in good agreement with the APM at all scales. The current SDSS sampling (1-sigma) errors range from 10% at scales of arc-minutes (less than 1 Mpc/h) to about 50% on degree scales (~ 10 Mpc/h). At this level both surveys are in perfect agreement. The collapse 3-point function, c_{12} shows even smaller errors (this is because multi-point statistics are better sampled over narrow strips than counts in large smoothed cells). At degree scales we find $c_{12} \simeq 2.2 \pm 0.4$. Its shape and amplitude is remarkably similar to what is found in simulations and theoretically expected from gravitational instability (see Bernardeau 1996, Gaztañaga, Fosalba & Croft 2001). The 3-point function for isosceles triangles of side $\theta_{12} = \theta_{13} = 0.5$ deg. (left panel in Fig.7) seems lower than the APM values, but within the 2-sigma confidence level at any single point. Again here we would need of the covariance matrix to say more. In general, the Norther SDSS strip has higher amplitudes for the reduced skewness or 3-point function than the Southern strip.

We conclude that the SDSS seems in good agreement with the previous galaxy surveys, and thus with the idea that gravitational growth from Gaussian initial conditions is most probably responsible for the hierarchical structures we see in the sky (eg FG99, Scoccimarro etal 2001, and references therein).

The above agreement is encouraging and have tempted us to look into the detailed shape of $w_2(\theta)$ on small scales, where the uncertainties are smaller and errors from the APM are more reliable. On scales $0.1 < \theta < 1$ degrees, we find some indications from slight ($\simeq 20\%$) deviations from a simple power law. Fig.5 shows that the different SDSS samples have very similar slopes to the APM survey, which shows traces of a characteristic S-shape or inflection with a maximum slope. In hierarchical clustering models, the initial slope of $d \ln \xi / d \ln r$ is a smoothed decreasing function of the separation r . Projection effects can partially wash out this curve, but can not produce any inflection to the shape (at least if the selection function is also regular). In Gaztañaga & Juszkiewicz (2001 and references therein) it was argued and shown that weakly non-linear evolution produces a characteristic S-shape in $d \ln \xi / d \ln r$. This shape, smoothed by projections, is also evident in the APM data for $d \ln w(\theta) / d \ln \theta$. Here we also find some evidence for such a shape in the combined EDR/(N+S) SDSS data. The maximum in the slope occurs around $\theta \simeq 0.7$ deg, which corresponds to $r \sim 5$ Mpc/h, as expected if biasing is small on those scales. Thus both the shape of the 2-point function and the shape and amplitude of the 3-point function and skewness in the SDSS EDR confirm that galaxies seem to be tracing a large scale distribution that started from Gaussian initial conditions (see Peebles 1980, Fry 1984, Juszkiewicz, Bouchet & Colombi 1993, Fry & Gaztañaga 1993, Gaztañaga 1994,

Bernardeau 1994, Fosalba & Gaztañaga 1998, Buchalter, Jaffe & Kamionkowski 2000, Scoccimarro et al. 2001, and references therein).

ACKNOWLEDGMENTS

I acknowledge support by grants from IEEC/CSIC and DGI/MCT BFM2000-0810. Funding for the creation and

distribution of the SDSS Archive has been provided by the Alfred P. Sloan Foundation, the Participating Institutions, the National Aeronautics and Space Administration, the National Science Foundation, the U.S. Department of Energy, the Japanese Monbukagakusho, and the Max Planck Society. The SDSS Web site is <http://www.sdss.org/>.

REFERENCES

- Bernardeau, F., 1994, *A&A* 291, 697
 Bernardeau, F., 1996, *A&A*, 312, 11 (B96)
 Buchalter, A., Jaffe, A., Kamionkowski, M., 2000, *ApJ*, 530, 36
 Connolly et al 2001, astro-ph/0107417
 Colombi, S., Szapudi, I., Jenkins, A., Colberg, J., 2000, *MNRAS* 313, 711
 Dodelson, S., Narayanan, V.K., Tegmark, M, Scranton, R., et al astro-ph/0107421, submitted to *ApJ*.
 Fosalba, P. & Gaztañaga, E., 1998, *MNRAS* 301, 503
 Frieman, J.A., Gaztañaga, E., 1999, *ApJ*, 521, L83 (FG99)
 Fry, J. N. 1984, *ApJ*, 279, 499
 Fry, J. N. & Gaztañaga, E. 1993, *ApJ*, 413, 447
 Gaztañaga, E., 2001, submitted to *MNRAS*, astro-ph/0107523 (G01)
 Gaztañaga, E., 1994, *ApJ*, 454, 561
 Gaztañaga, E., 1995, *MNRAS*, 268, 913
 Gaztañaga, E., & Baugh, C.M. 1998, *MNRAS*, 294, 229
 Gaztañaga, E. & Dalton, G.B., 2000, *MNRAS*, 312, 417
 Gaztañaga, E. & R. Juszkiewicz, 2001, *R. ApJ*, 558, L1
 Gaztañaga, E., Fosalba, P. & Croft, R., 2001, submitted to *MNRAS* astro-ph/0107523
 Hui, L. & Gaztañaga, E., 1999, *ApJ*, 519, 622
 Jenkins, A. et al 1998, *ApJ* 499, 20
 Juszkiewicz, R., Bouchet, F., & Colombi, S. 1993, *ApJ*, 412, L9
 Lupton, R., Gunn, J.E., Ivezić, Z Knapp, G.R., Kent, S., Yasuda, N, 2001, in ASP Conf. Ser. 238, *Astronomical Data Analysis Software and Systems X*, ed. F.R. Harnden, F.A. Primi and H.E. Payne, in press astro-ph/0101420
 Maddox, S.J., Efstathiou, G., Sutherland, W.J. & Loveday, J., 1990, *MNRAS*, 242, 43P
 Peebles, P.J.E., 1993, *Principles of Physical Cosmology*, Princeton University Press, Princeton
 Peebles, P.J.E., 1980, *The Large Scale Structure of the Universe*, Princeton: Princeton University Press
 Scoccimarro, R., Feldman, H., Fry, J. N. & Frieman, J.A., 2001 *ApJ*, 546, 652
 Scranton, R., Johnston, D., Dodelson, S., Frieman, J. et al astro-ph/0107416, submitted to *ApJ*.
 Szapudi, I., Dalton, G.B. , Efstathiou, G. & Szalay, A.S., 1995, *ApJ* 444, 520
 Szapudi, I. & Gaztañaga, E., 1998, *MNRAS* 300, 493
 Szapudi, I., & Szalay, A.S., 1999, *ApJ*, 515 L43
 Szalay, A.S. et al 2001, astro-ph/0107419
 Tegmark, M., Hamilton, A.J.S., Strauss, M.A., Vogeley, M.S. & Szalay, A.S. 1998, *ApJ*, 499, 555
 Tegmark, M., et al 2001, astro-ph/0107418, submitted to *ApJ*.
 Yasuda, N., Fukugita, M., Narayanan, V.K. et al 2001 astro-ph/0105545, submitted to *ApJ*.
 York, D.G. et al, 2000, *A.J.*, 120, 1579 astro-ph/0006396